Oil Shale, 2023, Vol. 40, No. 2, pp. 133–150
doi: https://doi.org/10.3176/oil.2023.2.03
ISSN 0208-189X

Determination of some physico-thermal and mechanical characteristics of hydrated Jordanian Lajjun oil shale ash

Ali Shawabkeh[(a)*], Fatemah Alansari[(a)], Djamel Ghernaout[(b,c)], Noureddine Elboughdiri[(b,d)]

[(a)] College of Engineering and Technology, American University of the Middle East, Kuwait
[(b)] Chemical Engineering Department, College of Engineering, University of Ha'il, P.O. Box 2440, Ha'il 81441, Saudi Arabia
[(c)] Chemical Engineering Department, Faculty of Engineering, University of Blida, P.O. Box 270, Blida 09000, Algeria
[(d)] Chemical Engineering Process Department, National School of Engineers Gabes, University of Gabes, Street Omar ibn El-Khattab, 6029 Gabes, Tunisia

Received 25 December 2022, accepted 14 April 2023, available online 10 May 2023

Abstract. *The hydration of oil shale ash at different water-to-ash weight (W/A) ratios ranging from 0.4 to 0.8 was experimentally investigated. The ash hydrate's physical characteristics, its particles' elemental composition, and the existing crystalline phases were identified using N_2 Brunauer-Emmerich-Teller (N_2-BET), Energy Dispersive X-ray (EDX) and X-ray Powder Diffraction (XRD) measurement techniques. The formed hydration cementitious products were found to be stratlingite ($2CaO{\cdot}Al_2O_3{\cdot}SiO_2{\cdot}8H_2O$), ettringite ($6CaO{\cdot}Al_2O_3{\cdot}3SiO_3{\cdot}32H_2O$), and melilite ($2CaO{\cdot}Al_2O_3{\cdot}SiO_2$) in the oil shale ash hydrated at W/A = 0.6. These same phases with different relative amounts were found in the oil shale ash hydrated at W/A = 0.8 in addition to calcium silicate hydrates (CSH). The drop in the physico-thermal properties (bulk density and thermal conductivity) of the hydrated ash was attributed to the formation of cementitious products, mainly to stratlingite, melilite, and ettringite. The hydrated ash's mechanical properties (bending and compressive strengths) were found to increase at higher W/A due to the formation of cementing materials, particularly CSH.*

Keywords: *hydration, pozzolan, compressive strength, bending strength, oil shale ash, calcium silicate hydrate.*

* Corresponding author: e-mail *Ali.Shawabkeh@aum.edu.kw*

1. Introduction

The world's known oil shale reserves are vast, being many times greater than the proven remaining resources of crude oil and natural gas [1]. Oil shale can be used as an energy source by retorting or direct combustion; however, both produce tremendous ash residue. The direct discharge of oil shale from the Jordanian Lajjun deposit for electric power generation often evolves 52 to 57 wt% ash [2, 3] and thus causes severe environmental pollution and disposal problems unless correctly performed. There are different ways to utilize ash wastes, such as the well-developed technology using coal-derived fly ash and lime (CaO) in pavements, buildings, and bridge construction [4]. Al-Shawabkeh et al. [5, 6] have, moreover, shown that active sorbents for sulfur dioxide capture could be prepared by special treatment of fly ashes from both atmospheric fluidized-bed combustors and pulverized coal combustors. Usta et al. [7] mentioned that some types of ash could be used as a potential independent binder. However, they also claimed that other types of fly ash could require additional physical or thermal pre-treatments to make them fit for cement and concrete applications. Raado et al. [8] concluded that the high content of free CaO causes domination of quick lime-type hydration. Furthermore, they reported that the hydration process resulted in ettringite formation due to a sufficient amount of $Ca(OH)_2$, followed by hydraulic reactions of calcium silicates and water. Mõtlep et al. [9] found that the ash left after burning kerogenous Estonian oil shale was composed of lime, anhydrite, Ca-silicate mineral phases, and X-ray amorphous Al-Si glass phase, which were unstable under open atmospheric and wet conditions, and become hydrated into metastable secondary phases portlandite (calcite), gypsum, ettringite, and hydrocalumite. Kuusik et al. [10] reported that hydrated ash contained different complex compounds, such as calcium silicate hydroxide hydrate $Ca_4{\cdot}5Si_6O_{15}(OH)_3{\cdot}2H_2O$ that represents silicates; besides, calcium aluminum oxide carbonate hydrate $Ca_6Al_2O_6(CO_3)_3{\cdot}32H_2O/3CaO{\cdot}Al_2O_3{\cdot}3CaCO_3{\cdot}32H_2O$ and calcium aluminum oxide sulfate $Ca_4Al_6O_{12}(SO_4)/3CaO{\cdot}3Al_2O_3{\cdot}CaSO_4$ are present. Further, calcium aluminum iron oxide hydroxide $Ca_{12}Al_{13}{\cdot}8Fe0.14O_{32}(OH)_2/11CaO{\cdot}6.9Al_2O_3{\cdot}0.07Fe_2O_3{\cdot}Ca(OH)_2$, brownmillerite $Ca_2(Al,Fe)_2O_5$ and calcium aluminum iron oxide $CaA_{18}Fe_4O_{19}/CaO{\cdot}4Al_2O_3{\cdot}2Fe_2O_3$ are present as Ca, Fe and Al compounds. Moreover, aluminum hydroxide $Al(OH)_3$ as nordstrandite or vesuvianite ferrian $Ca_{19}(Al,Mg,Fe)_{11}(Si,Al)_{18}O_{69}(OH)_2$ is found. During the open-air hydration of circulating fluidized bed combustion oil shale ash, Liira et al. [11] noted (1) a rapid free lime hydration into the portlandite reaction, which was completed in oil shale ash in 72 h; (2) the dissolution of anhydrite and periclase in 144 h; (3) a delayed, yet rapid formation of (crystalline) ettringite after 144 h and (4) a slow carbonation of portlandite and decomposition of ettringite into calcite and Ca-sulphate hemihydrate (bassanite) when pH decreases below 10.7 after portlandite has converted to stable calcite.

Jozewicz et al. [12] reported that $CaO\text{-}Al_2O_3\text{-}SiO_2\text{-}CaSO_4\text{-}H_2O$ yielded cementitious phases originating from the pozzolanic reaction of lime with fly ash or clay. Likewise, Torrey [13] utilized coal fly ash to produce thermal insulation bricks in a process involving wet mixing of the ingredients of 77 wt% fly ash, 20 wt% lime, 3 wt% gypsum, and aluminum powder. The coal-derived ash, thus, requires at least lime and gypsum addition during hydrothermal treatment to undergo pozzolanic reactions with other siliceous or siliceous and aluminous material in the presence of water to form cementitious compounds.

Different from coal ash, oil shale ash possesses pozzolanic activity as well as hydraulic properties due to its high content of free lime and sulfur trioxide (SO_3), and, therefore, it can develop hardness with water with no need for further additives [3, 14, 15]. The present work, therefore, was aimed at investigating the hydration effect on some physico-thermal (bulk density and thermal conductivity) and mechanical properties (bending and compressive strengths) of oil shale ash containing considerable amounts of free lime (26.2%) and anhydrite.

2. Experimental method

2.1. Oil shale

The oil shale samples utilized in this work were collected from the Lajjun deposit in the central coastal part of Jordan. Fischer assay analysis (wt%) showed Lajjun oil shale to contain 11% oil, 80.61% spent shale, 4% moisture and 4.39% off-gases. Table 1 presents the chemical composition of dried Lajjun oil shale and Estonian oil shale [16]. Both Jordanian and Estonian oil shales have an equal amount of mineral CO_2, indicating the high content of carbonates such as calcite and dolomite. It is worth mentioning that Lajjun oil shale has a higher sulphur content in its organic part compared with Estonian oil shale. The amount of sulphur in Lajjun shale oil and in original oil shale was found to range from 7 to 9.5 wt% [17]. This fact adds environmental and economic restrictions to the future utilization of Jordanian oil shale.

Table 1. Chemical composition of Jordanian and Estonian oil shales, wt%, dry

Component	Lajjun oil shale	Estonian oil shale
Ash	57.19	50.5
CO_2 (mineral)	19.75	19.8
Total S	3.26	1.63
Organic C	15.56	28.3

Table 1 (continued)

Component	Lajjun oil shale	Estonian oil shale
H	3.43	3
N	0.80	0.53
O	1.96	–

2.2. Ashing, ash particle size distribution and composition

The oil shale samples were combusted in the laboratory-scale batch-loaded fluidized bed reactor at temperatures ranging from 750 to 830 °C. The ashing for the as-collected oil shale ash discharged from the reactor was conducted by placing it in an oven (carbolite furnace) and kept at a constant temperature of 200 °C (heating rate 10 °C/min) for one day to dry before use with no special pretreatment. Then the ash was ground and sieved less than 52 μm in diameter. The particle size distribution of a random ash sample is shown in Figure 1. This size distribution represents the actual one obtained after the ashing process and before the hydration process. Therefore, it may differ from the size distribution of the ash derived from the direct oil shale combustion in the fluidized bed reactor.

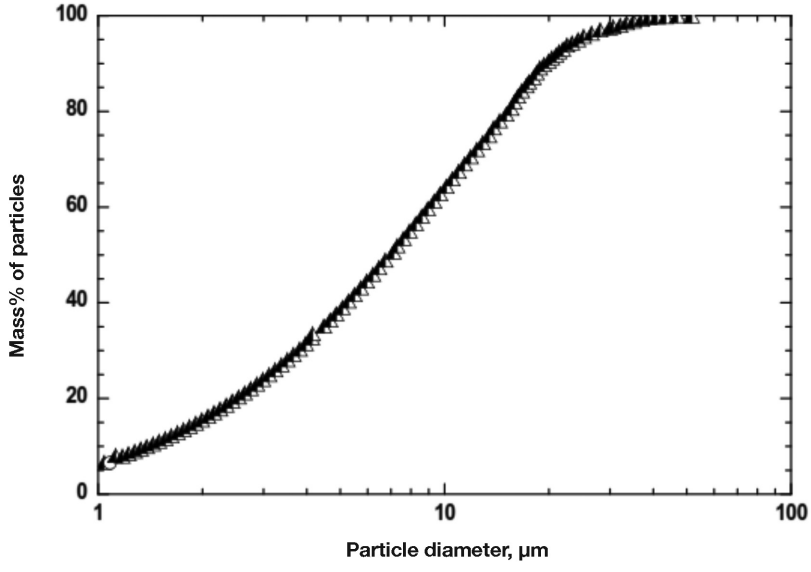

Fig. 1. Particle size distribution in the Lajjun oil shale ash.

The particle diameter ranged from 1 to 52 μm, and the mass median particle diameter was 7.4 μm. The dried ash samples were also analyzed by X-ray Powder Diffraction (XRD) in the Laboratories Directorate of the Natural Resources Authority (Amman, Jordan) to determine their chemical composition. Table 2 reveals the chemical composition of Jordanian and Estonian oil shale ashes (on dry basis). The Estonian pulverized firing cyclone ash (PF/CA) was collected from a pulverized-firing cyclone [16]. The fact that the Jordanian ash contained a higher amount of SO_3 (13.06 wt%) compared to the Estonian ash (3.4 wt% SO_3) could indicate the formation of more ettringite during ash hydration. Both Jordanian and Estonian ashes contained relatively significant amounts of alumina (5.58 and 6.4%, respectively) and silica (19.53 and 24.5%, respectively) which are essential for the pozzolanic reaction and strength gain.

Table 2. Chemical composition of Jordanian and Estonian oil shale ashes, wt%, dry

Component	Lajjun ash	Estonian ash (PF/CA)
CaO (total)	51.43	51.6
CaO (free)	26.2	22.7
SiO_2	19.53	24.5
SO_3	13.06	3.4
Al_2O_3	5.58	6.4
P_2O_5	4.34	–
Fe_2O_3	3.72	3.9
MgO	1.59	4.9
Na_2O	0.53	0.14
TiO_2	0.17	–
MnO	0.04	–
K_2O	0.01	2

2.3. Oil shale ash paste manufacturing method and characterization

The ash paste was prepared by slurring the dried ash with deionized water inside a vessel agitated at 160 revolutions per minute (rpm) for 7 min. The initial hydration of the ash resulted in mix temperatures exceeding 100 °C due to the exothermic reactions of water with the ash-free lime and, to a lesser extent, with calcium sulfate ($CaSO_4$). Therefore, the 7-min hydration period minimizes this undesirable temperature rise. The added deionized water-to-solid ash weight (W/A) ratios varied from 0.4 to 0.8. The paste was slowly poured into a wooden rectangular mold with a length, width and depth of 6.0, 4.5, and 2.0 cm, respectively, without any need for vibration. It was then pressed (simple compaction) during the pouring process. A bigger mold size of 10.0 cm × 8.0 cm × 2.0 cm was tested at the beginning of this work, and no profound effect on the obtained findings was observed within 5 to 7% errors. The mold was then placed in a humidity-controlled chamber (Tabai Labostar, ESPEC LH-112T) for curing at 75% relative humidity and 80 °C for about three days. All the paste samples were prepared in the same fashion (pouring and pressing), and the physico-thermal and mechanical tests were repeated 2 to 3 times for each sample. The accepted accuracy of the obtained measurement results (within 4%) emphasized that sticking to the pouring/compaction fashion in this work was fair and adequate.

The hydrate crystalline and glassy phases were determined using an X-ray powder diffractometer (Rigaku XRD). Next, the bulk density was determined by measuring the brick weight and volume, and the thermal conductivity was measured by a Quick Thermal Conductivity Meter (QTM-500, Kyoto Denshi Kyogyoo Kabushikigaisha). Finally, the mechanical properties (bending and compressive strengths) were measured with a tensile-compressive tester (Imada Factory, Load Tester Type SV55, Toyohashi, Japan).

3. Results and discussion

3.1. Nitrogen-Brunauer-Emmett-Teller physisorption analysis

The important pore characteristics of the ash before and after hydration were determined from the nitrogen (N_2) absorption-desorption isotherms using the Brunauer-Emmett-Teller (BET) theory based on measurements with the accelerated surface area and porosimetry analyzer (ASAP 2020, Norcross, Georgia, USA). Table 3 lists the measured micro results as the specific surface area and specific pore volume.

A rough comparison between the generated figures indicates a significant improvement in the specific surface area and pore volume of the hydrated ash samples. For example, during ash hydration (at W/A = 0.8), the specific surface area and the cumulative pore volume increased over five times; such increase indicates the formation of micropores in the existing hydration

Table 3. Pore characteristics of original and hydrated ash samples

W/A	Specific surface area S_p, m^2/g	Specific cumulative pore volume V_p, mm^3/g
0 (original oil shale ash)	5.82	29
0.6	34.36	174
0.8	36.18	193

products (calcium silicates and calcium aluminates), which are known to possess large surface area and porosity [18–20].

3.2. X-ray Powder Diffraction and Energy Dispersive X-ray analyses

For the qualitative X-ray Powder Diffraction (XRD) and Energy Dispersive X-ray (EDX) analyses of the ash samples before and after hydration, the X-ray patterns and assignment of the peaks in the original (unhydrated) and hydrated ash samples are given in Figure 2. The mineralogical composition of the original ash mainly includes crystalline compounds quartz (SiO_2), anhydrite ($CaSO_4$), calcite ($CaCO_3$), free lime (CaO), and periclase (MgO).

An amorphous halo appeared between the angular zone (2Θ) of 20°–55°, which corresponds to the glassy component of ash. In the ash hydrated at W/A = 0.6, the quartz reflection peaks disappeared entirely during the hydration reaction while relative amounts of calcite, lime, periclase, and anhydrite remained in the hydrated product. Thus, for this 0.6 ash, the formed hydration phases were identified to be stratlingite ($2CaO{\cdot}Al_2O_3{\cdot}SiO_2{\cdot}8H_2O$), ettringite ($6CaO{\cdot}Al_2O_3{\cdot}3SO_3{\cdot}32H_2O$), and melilite ($2CaO{\cdot}Al_2O_3{\cdot}SiO_2$). At a 0.8 hydration ratio, both quartz and lime peaks disappeared entirely during the hydration reaction. In contrast, new peaks of calcium silicate hydrates were detected in addition to stratlingite, ettringite, and melilite at different relative amounts. CSH and ettringite formed due to the hydration of a mix of coal fly ash, lime, and anhydrite, as reported by Tsuchiai et al. [21].

To quantitatively determine the current phases, an energy-dispersive X-ray analyzer (Superscan SSX-550 SEM-EDX, Shimadzu) was used to provide elemental identification and quantitative compositional information. The amounts of elements in different regions in the ash were analyzed to determine the type of phases formed in the hydrated sample.

The results for individual EDX microanalyses from variable regions (3 to 5 areas per scanning electron microscopy (SEM) photo) of the 0.6 and 0.8 ash samples (ash samples hydrated at W/A of 0.6 and 0.8) are presented in Table 4 as calculated from the quantitative analysis of the EDX spectra. (Details of the calculation are shown in the Supporting Information).

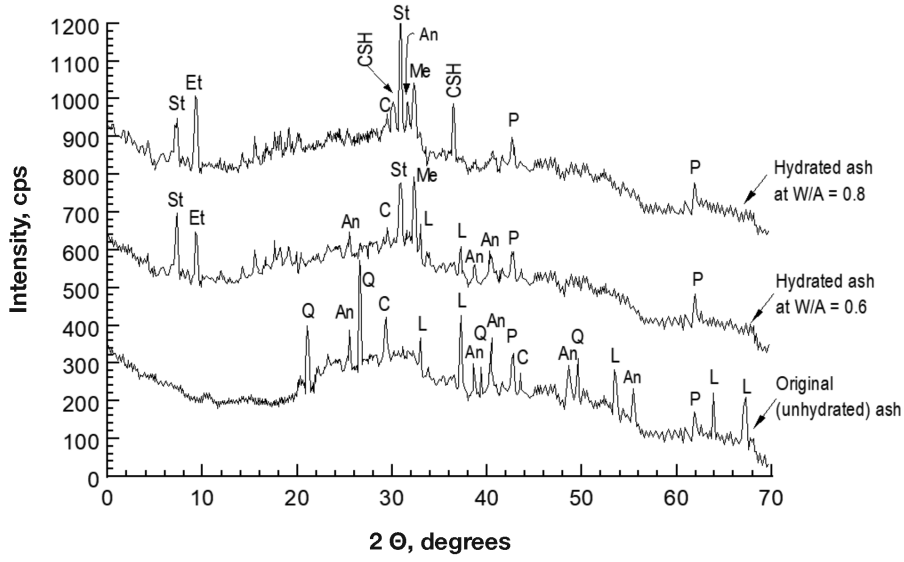

Fig. 2. X-ray diffraction patterns of original (unhydrated) oil shale ash and hydrated ash samples (An – anhydrite, C – calcite, Q – quartz, L – lime, P – periclase, Me – melilite, St – stratlingite, Et – ettringite).

Average Si/Ca and Al/Ca atom ratios of 0.463 and 0.976, respectively, were found in the 0.6 ash (Analysis Group 1 in Table 4) and 0.488 and 0.813, respectively, for the 0.8 ash (Analysis Group 2). The mean unit formula compositions were calculated as follows: $2CaO{\cdot}Al_2O_3{\cdot}SiO_2$: $Si_{0.859}{\cdot}Al_{1.809}{\cdot}Fe_{0.074}{\cdot}S_{0.163}Ca_{1.854}{\cdot}Na_{0.023}{\cdot}P_{0.042}{\cdot}Mg_{0.028}{\cdot}Ti_{0.000}{\cdot}O_7$ for 0.6 ash, and $Si_{0.988}{\cdot}Al_{1.645}{\cdot}Fe_{0.066}{\cdot}S_{0.103}{\cdot}Ca_{2.024}{\cdot}Na_{0.019}{\cdot}P_{0.020}{\cdot}Mg_{0.018}{\cdot}Ti_{0.001}{\cdot}O_7$ for 0.8 ash. These findings compare well with the ideal Si/Ca and Al/Ca atom ratios for the XRD-detected compounds, which were found to be 0.5 and 1.0 for stratlingite ($2CaO{\cdot}Al_2O_3{\cdot}SiO_2{\cdot}8H_2O$) and melilite ($2CaO{\cdot}Al_2O_3{\cdot}SiO_2$), respectively.

The mean unit formula compositions were calculated as $2CaO{\cdot}Al_2O_3{\cdot}SiO_2$ (Analysis Groups 4 and 5 in Table 4): $Si_{0.179}{\cdot}Al_{1.324}{\cdot}Fe_{0.315}{\cdot}S_{2.302}{\cdot}Ca_{5.192}{\cdot}Na_{0.042}{\cdot}P_{0.249}{\cdot}Mg_{0.100}{\cdot}Ti_{0.001}{\cdot}O_{18}$ for 0.6 ash, and $Si_{0.209}{\cdot}Al_{1.545}{\cdot}Fe_{0.153}{\cdot}S_{2.746}{\cdot}Ca_{4.880}{\cdot}Na_{0.019}{\cdot}P_{0.020}{\cdot}Mg_{0.018}{\cdot}Ti_{0.001}{\cdot}O_{18}$ for 0.8 ash. This is in good agreement with the ideal S/Ca and Al/Ca atom ratios for the XRD-detected compounds, which were found to be 0.5 and 0.33 for ettringite ($6CaO{\cdot}Al_2O_3{\cdot}3SO_3{\cdot}32H_2O$).

The mean unit formula composition was calculated as $0.8–1.5(CaO){\cdot}SiO_2{\cdot}1–2.5(H_2O)$ (Analysis Group 3 in Table 4): $Si_{0.893}{\cdot}Al_{0.132}{\cdot}Fe_{0.032}{\cdot}S_{0.043}{\cdot}Ca_{1.273}{\cdot}Na_{0.019}{\cdot}P_{0.020}{\cdot}Mg_{0.018}{\cdot}Ti_{0.001}{\cdot}O_{3.5}$ only for 0.8 ash, which compares well with the ideal Si/Ca atom ratios for the XRD-detected compounds found to be between 0.67 and 1.25 for CSH: $0.8–1.5(CaO){\cdot}SiO_2{\cdot}1–2.5(H_2O)$.

From the above qualitative and quantitative analysis, we can conclude that the hydration of oil shale ash resulted in the formation of stratlingite, melilite, and ettringite (for 0.6 ash), and stratlingite, melilite, ettringite, and new CSH (for 0.8 ash).

Table 4. Compositions of oxides and elements in the main regions of hydrated ash calculated from EDX analysis

Analysis Group*	Sample	Oxides	SiO_2	Al_2O_3	Fe_2O_3	SO_3	CaO	Na_2O	P_2O_5	MgO	TiO_2	Total
1	Ash hydrated at 0.6	wt%	19.47	34.81	2.02	4.93	39.23	0.24	1.02	0.39	0.01	102.1
		Elements	**Si**	**Al**	**Fe**	**S**	**Ca**	**Na**	**P**	**Mg**	**Ti**	
		wt%	9.101	18.424	1.413	1.974	28.038	0.178	0.445	0.235	0.006	
		mol%	0.324	0.683	0.025	0.062	0.700	0.008	0.014	0.010	0.000	
		Mean molar ratios relative to Ca	0.463	0.976	0.036	0.088	1.000	0.011	0.021	0.014	0.000	
2	Ash hydrated at 0.8	wt%	19.47	34.81	2.02	4.93	39.23	0.24	1.02	0.39	0.01	102.1
		Elements	**Si**	**Al**	**Fe**	**S**	**Ca**	**Na**	**P**	**Mg**	**Ti**	
		wt%	10.312	16.502	1.294	1.230	30.160	0.260	0.380	0.265	0.019	
		mol%	0.367	0.612	0.023	0.038	0.753	0.011	0.012	0.011	0.000	
		Mean molar ratios relative to Ca	0.488	0.813	0.031	0.051	1.000	0.015	0.016	0.015	0.001	
3	Ash hydrated at 0.8	wt.%	39.17	4.91	1.85	2.53	52.12	0.35	0.870	0.44	0.032	102.3
		Elements	**Si**	**Al**	**Fe**	**S**	**Ca**	**Na**	**P**	**Mg**	**Ti**	
		wt%	18.310	2.599	1.294	1.013	37.250	0.260	0.380	0.265	0.019	
		mol%	0.652	0.096	0.023	0.032	0.929	0.011	0.012	0.011	0.000	
		Mean molar ratios relative to Ca	0.701	0.104	0.025	0.034	1.000	0.012	0.013	0.012	0.000	
4	Ash hydrated at 0.6	wt%	7.98	10.23	3.81	27.93	44.12	0.44	6.02	1.38	0.03	101.9
		Elements	**Si**	**Al**	**Fe**	**S**	**Ca**	**Na**	**P**	**Mg**	**Ti**	
		wt%	3.730	5.414	2.665	11.186	31.532	0.326	2.627	0.832	0.018	
		mol%	0.133	0.201	0.048	0.349	0.787	0.014	0.085	0.034	0.000	
		Mean molar ratios relative to Ca	0.169	0.255	0.061	0.443	1.000	0.018	0.108	0.044	0.000	
5	Ash hydrated at 0.8	wt%	9.17	11.9	1.85	33.21	41.34	0.35	0.870	0.44	0.032	99.2
		Elements	**Si**	**Al**	**Fe**	**S**	**Ca**	**Na**	**P**	**Mg**	**Ti**	
		wt%	4.286	6.298	1.294	13.301	29.546	0.260	0.380	0.265	0.019	
		mol%	0.153	0.233	0.023	0.415	0.737	0.011	0.012	0.011	0.000	
		Mean molar ratios relative to Ca	0.207	0.317	0.031	0.563	1.000	0.015	0.017	0.015	0.001	

* The group included 3 to 4 spots

3.3. Physico-thermal properties of produced hydrate

3.3.1. Thermal conductivity

The relationship between the bulk density of hydrated ash and the W/A ratio is depicted in Figure 3. The hydrated ash decreased the density from 1216 kg/m^3 at W/A of 0.4 to 1132 kg/m^3 at W/A of 0.8.

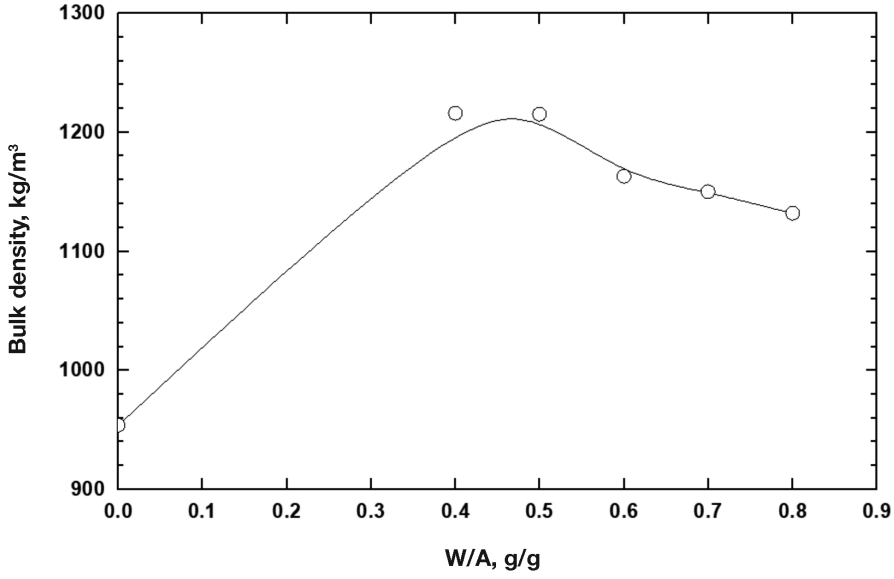

Fig. 3. Change of bulk density of hydrated oil shale ash with water-to-ash weight ratio (W/A).

The thermal conductivity, as seen from Figure 4, was also found to decrease from 0.241 W/m·K to 0.124 W/m·K with W/A increasing from 0.4 to 0.8. The associated reduction in thermal conductivity with density decrease was reported by many researchers [8, 22–29]. The main reason for the decline in bulk density and thermal conductivity is the porous nature of the pozzolanic products in the treated ash (the hydration reactions), in addition to the more porous structure developed through the slow water evaporation rate (dehydration) during the three days of the curing period.

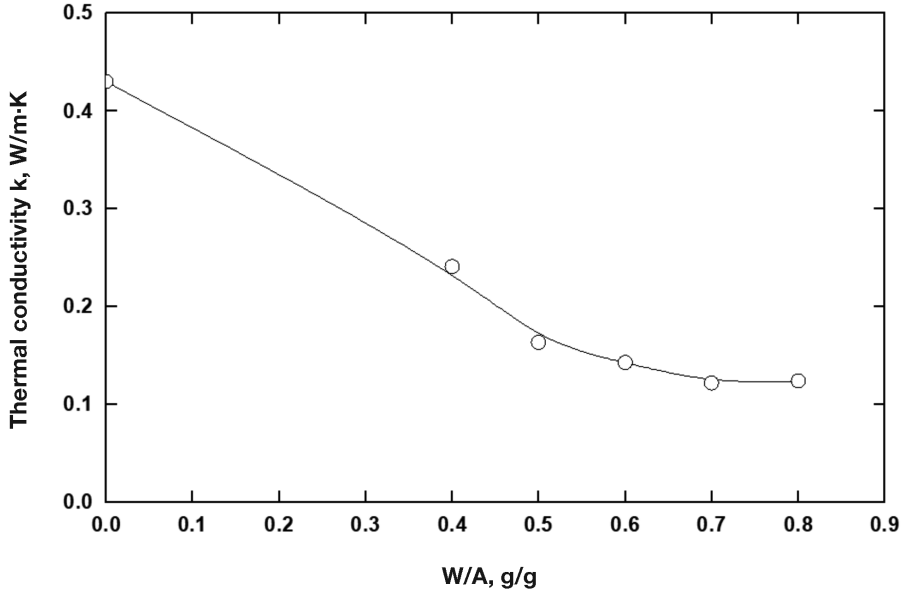

Fig. 4. Variation of the thermal conductivity k of hydrated oil shale ash with water-to-ash weight ratio (W/A).

The thermal conductivity values obtained in this work for the 0.6 to 0.8 hydrated samples were in the range of 0.12–0.14 W/m·K. Though the associated densities were within 1132–1163 kg/m^3, the other properties of the hydration phases formed, such as the specific surface area and pore volume, are most probably responsible for the relatively low thermal conductivities attained.

3.3.2. Mechanical properties

The variations of the bending and compressive strengths with W/A are shown in Figure 5. Increasing the hydration ratio (i.e., W/A) from 0.4 to 0.8 resulted in approximately 60% and 100% increases in the compressive and bending strengths, respectively. Maximum bending and compressive strengths of 1.97 and 3.47 MPa could be attained at a hydration ratio of 0.8. The strength gain of the hydrated fly ash was related to the formation of CSH and partly to the formed ettringite network (needles) in the early hydration time when the ash anhydrite reacts with aluminate and lime [4].

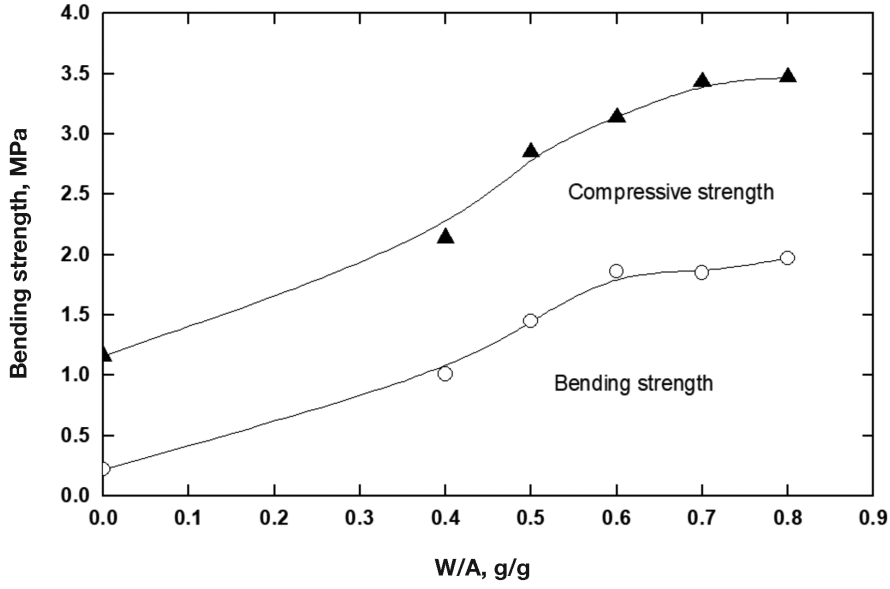

Fig. 5. Variation of the bending and compressive strengths of hydrated oil shale ash with water-to-ash weight ratios.

The ettringite formation from the hydration of ash is not unexpected with the relatively high anhydrite amount in the Lajjun oil shale ash (13.06 wt% SO_3, Table 2). The hydrated calcium silicates and aluminates were found to be mainly responsible for strength development in both cement-hardening reactions and pozzolanic reactions [30]. The 6% and 11% increase in the bending and compressive strengths of the 0.8 ash relative to that of the 0.6 ash is most likely ascribed to the CSH phase in the 0.8 ash.

Soon, the first oil shale-based power plant will start operation in Jordan. The desired massive ash will discharge and accumulate on the plant's site. During the rainy season, the ash constituents' leachability process will occur, and the leachate is expected to contaminate the ground and water surfaces. However, due to the limited work on the effect of oil shale ash on the environment [31–33] much more research work will be necessary.

4. Conclusions

The hydration of oil shale ash at different water-to-ash weight ratios ranging from 0.4 to 0.8 was experimentally investigated. The pozzolanic reaction between the hydrated ash constituents resulted in the following:

- formation of hydration cementitious products (stratlingite, ettringite, and melilite) in the ash hydrated at W/A = 0.6;

- formation of calcium silicate hydrates in addition to stratlingite, ettringite, and melilite in the ash hydrated at W/A = 0.8;
- formation of stratlingite, melilite, and ettringite assumed to be responsible for the drop in the bulk density and thermal conductivity of the hydrated ash;
- higher increase of the bending and compressive strengths of the hydrated ash at higher W/A due to the formation of cementing materials, particularly calcium silicate hydrates.

Finally, it should be noted that the above results are valid only for the Jordanian Lajjun oil shale burnt under certain conditions, i.e. burning at 750 to 830 °C inside a laboratory-scale batch-loaded fluidized bed reactor, and its derived ash prepared in conditions close to those mentioned in the current work.

Acknowledgment

The publication costs of this article were partially covered by the Estonian Academy of Sciences.

REFERENCES

1. Wang, Q., Sun, B., Wu, X., Bai, J., Sun, J. Study on combustion characteristics of mixtures of Huadian oil shale and semicoke. *Oil Shale*, 2007, **24**(2), 135–145. https://doi.org/10.3176/oil.2007.2.04
2. Kaljuvee, T., Jefimova, J., Loide, V., Uibu, M., Einard, M. Influence of the post-granulation treatment on the thermal behaviour and leachability characteristics of Estonian oil shale ashes. *J. Therm. Anal. Calorim.*, 2018, **132**(1), 47–57. https://doi.org/10.1007/s10973-017-6875-2
3. Kuusik, R., Uibu, M., Kirsimäe, K. Characterization of oil shale ashes formed at industrial-scale CFBC boilers. *Oil Shale*, 2005, **22**(4S), 407–419. https://doi.org/10.3176/oil.2005.4s.04
4. Hadi, N. A. R. A., Abdelhadi, M. Characterization and utilization of oil shale ash mixed with granitic and marble wastes to produce lightweight bricks. *Oil Shale*, 2018, **35**(1), 56–69. https://doi.org/10.3176/oil.2018.1.04
5. Al-Shawabkeh, A., Matsuda, H., Hasatani, M. Utilization of highly improved fly ash for SO_2 capture. *J. Chem. Eng. Japan*, 1995, **28**(1), 53–58. https://doi.org/10.1252/jcej.28.53
6. Al-Shawabkeh, A., Maisuda, H., Hasatani, M. Comparative reactivity of treated FBC- and PCC-fly ash for SO_2 removal. *Can. J. Chem. Eng.*, 1995, **73**(5), 678–685. https://doi.org/10.1002/cjce.5450730511
7. Usta, M. C., Yörük, C. R., Hain, T., Paaver, P., Snellings, R., Rozov, E., Gregor, A., Kuusik, R., Trikkel, A., Uibu, M. Evaluation of new applications of

oil shale ashes in building materials. *Minerals*, 2020, **10**(9), 1–19. https://doi.org/10.3390/min10090765

8. Raado, L.-M., Kuusik, R., Hain, T., Uibu, M., Somelar, P. Oil shale ash based stone formation - hydration, hardening dynamics and phase transformations. *Oil Shale*, 2014, **31**(1), 91–101. https://doi.org/10.3176/oil.2014.1.09
9. Mõtlep, R., Sild, T., Puura, E., Kirsimäe, K. Composition, diagenetic transformation and alkalinity potential of oil shale ash sediments. *J. Hazard. Mater.*, 2010, **184**(1–3), 567–573. https://doi.org/10.1016/j.jhazmat.2010.08.073
10. Kuusik, R., Paat, A., Veskimäe, H., Uibu, M. Transformations in oil shale ash at wet deposition. *Oil Shale*, 2004, **21**(1), 27–42. https://doi.org/10.3176/oil.2004.1.04
11. Liira, M., Kirsimäe, K., Kuusik, R., Mõtlep, R. Transformation of calcareous oil-shale circulating fluidized-bed combustion boiler ashes under wet conditions. *Fuel*, 2009, **88**(4), 712–718. https://doi.org/10.1016/j.fuel.2008.08.012
12. Jozewicz, W., Chang, J. C. S., Brna, T. G., Sedman, C. B. Reactivation of solids from furnace injection of limestone for sulfur dioxide control. *Environ. Sci. Technol.*, 1987, **21**(7), 664–670. https://doi.org/10.1021/es00161a007
13. *Coal Ash Utilization: Fly Ash, Bottom Ash and Slag 1978* (Torrey, S., ed.). NJ, Noyes Data Corporation, 1978. https://doi.org/10.1016/0361-3658(81)90030-8
14. Aljbour, S. H. Production of ceramics from waste glass and Jordanian oil shale ash. *Oil Shale*, 2016, **33**(3), 260–271. https://doi.org/10.3176/oil.2016.3.05
15. Irha, N., Uibu, M., Jefimova, J., Raado, L.-M., Hain, T., Kuusik, R. Leaching behaviour of Estonian oil shale ash-based construction mortars. *Oil Shale*, 2014, **31**(4), 394–411. https://doi.org/10.3176/oil.2014.4.07
16. Kaljuvee, T., Uibu, M., Yörük, C. R., Einard, M., Trikkel, A., Kuusik, R., Trass, O., Štubňa, I., Húlan, T., Loide, V., Jefimova, J. Study of thermooxidation of oil shale samples and basics of processes for utilization of oil shale ashes. *Minerals*, 2021, **11**(2), 193. https://doi.org/10.3390/min11020193
17. Al-Harahsheh, A., Al-Otoom, A. Y., Shawabkeh, R. A. Sulfur distribution in the oil fractions obtained by thermal cracking of Jordanian El-Lajjun oil shale. *Energy*, 2005, **30**(15), 2784–2795. https://doi.org/10.1016/j.energy.2005.01.013
18. Kaljuvee, T., Keelmann, M., Trikkel, A., Kuusik, R. Thermooxidative decomposition of oil shales. *J. Therm. Anal. Calorim.*, 2011, **105**(2), 395–403. https://doi.org/10.1007/s10973-010-1033-0
19. Marangoni, M., Ponsot, I., Kuusik, R., Bernardo, E. Strong and chemically inert sinter crystallised glass ceramics based on Estonian oil shale ash. *Adv. Appl. Ceram.*, 2014, **113**(2), 120–128. https://doi.org/10.1179/1743676113Y.0000000132
20. Trikkel, A., Keelmann, M., Kaljuvee, T., Kuusik, R. CO_2 and SO_2 uptake by oil shale ashes: Effect of pre-treatment on kinetics. *J. Therm. Anal. Calorim.*, 2010, **99**(3), 763–769. https://doi.org/10.1007/s10973-009-0423-7
21. Tsuchiai, H., Ishizuka, T., Ueno, T., Hattori, H., Kita, H. (1995). Highly active absorbent for SO2 removal prepared from coal fly ash. *Ind. Eng. Chem. Res.*, 1995, **34**(4), 1404–1411. https://doi.org/10.1021/ie00043a048

22. Balo, F., Ucar, A., Lütfi Yücel, H. Development of the insulation materials from coal fly ash, perlite, clay and linseed oil. *Ceram-Silikaty*, 2010, **54**(2), 182–191.
23. Blinova, I., Bityukova, L., Kasemets, K., Ivask, A., Käkinen, A., Kurvet, I., Bondarenko, O., Kanarbik, L., Sihtmäe, M., Aruoja, V., Schvede, H., Kahru, A. Environmental hazard of oil shale combustion fly ash. *J. Hazard. Mater.*, 2012, **229–230**, 192–200. https://doi.org/10.1016/j.jhazmat.2012.05.095
24. Demirboğa, R. Influence of mineral admixtures on thermal conductivity and compressive strength of mortar. *Energy Build.*, 2003, **35**(2), 189–192. https://doi.org/10.1016/S0378-7788(02)00052-X
25. Demirboğa, R. Thermo-mechanical properties of sand and high volume mineral admixtures. *Energy Build.*, 2003, **35**(5), 435–439. https://doi.org/10.1016/S0378-7788(02)00159-7
26. Kaljuvee, T., Štubňa, I., Húlan, T., Kuusik, R. Heating rate effect on the thermal behavior of some clays and their blends with oil shale ash additives. *J. Therm. Anal. Calorim.*, 2017, **127**(1), 33–45. https://doi.org/10.1007/s10973-016-5347-4
27. Khan, M. I. Factors affecting the thermal properties of concrete and applicability of its prediction models. *Build. Environ.*, 2002, **37**(6), 607–614. https://doi.org/10.1016/S0360-1323(01)00061-0
28. Konist, A., Neshumayev, D., Baird, Z. S., Anthony, E. J., Maasikmets, M., Järvik, O. Mineral and heavy metal composition of oil shale ash from oxyfuel combustion. *ACS Omega*, 2020, **5**(50), 32498–32506. https://doi.org/10.1021/acsomega.0c04466
29. Uysal, H., Demirboga, R., Şahin, R., Gül, R. The effects of different cement dosages, slumps, and pumice aggregate ratios on the thermal conductivity and density of concrete. *Cem. Concr. Res.*, 2004, **34**(5), 845–848. https://doi.org/10.1016/j.cemconres.2003.09.018
30. Kaljuvee, T., Štubňa, I., Somelar, P., Mikli, V., Kuusik, R. Thermal behavior of some Estonian clays and their mixtures with oil shale ash additives. *J. Therm. Anal. Calorim.*, 2014, **118**(2), 891–899. https://doi.org/10.1007/s10973-014-3797-0
31. Al-Adamat, R., Al-Harahsheh, A., Al-Farajat, M. The use of GIS and leachability tests to investigate groundwater vulnerability to pollution from oil shale utilization at Lajjoun area/Southern Jordan. *Jordan J. Civ. Eng.*, 2010, **4**(3), 253–263.
32. Al-Harahsheh, A., Al-Adamat, R., Al-Farajat, M. Potential impacts on surface water quality from the utilization of oil shale at Lajjoun area/Southern Jordan using geographic information systems and leachability tests. *Energ. Source. Part A*, 2010, **32**(19), 1763–1776. https://doi.org/10.1080/15567036.2010.491779
33. Al-Otoom, A. Y., Shawabkeh, R. A., Al-Harahsheh, A. M., Shawaqfeh, A. T. The chemistry of minerals obtained from the combustion of Jordanian oil shale. *Energy*, 2005, **30**(5), 611–619. https://doi.org/10.1016/j.energy.2004.05.024

Supporting Information

A. Calculation from the quantitative analysis of the EDX spectra (stratlingite and melilite)

Analysis Group	Ash hydrated at W/A of		SiO_2	Al_2O_3	Fe_2O_3	SO_3	CaO	Na_2O	P_2O_5	MgO	TiO_2		
1	0.6	wt%	19.47	34.81	2.02	4.93	39.23	0.24	1.02	0.39	0.01		
2	0.8	wt%	22.06	31.18	1.85	3.07	42.2	0.35	0.870	0.44	0.032		
			Si	Al	Fe	S	Ca	Na	P	Mg	Ti		
1	0.6	wt%	9.101	18.424	1.413	1.974	28.038	0.178	0.445	0.235	0.006		
		mol%	0.324	0.683	0.025	0.062	0.700	0.008	0.014	0.010	0.000		
		Mean molar ratios relative to Ca	0.463	0.976	0.036	0.088	1.000	0.011	0.021	0.014	0.000		
2	0.8	wt%	10.312	16.502	1.294	1.230	30.160	0.260	0.380	0.265	0.019		
		mol%	0.367	0.612	0.023	0.038	0.753	0.011	0.012	0.011	0.000		
		Mean molar ratios relative to Ca	0.488	0.813	0.031	0.051	1.000	0.015	0.016	0.015	0.001		
	Ash hydrated at W/A of		Calculated O from										
			SiO_2	Al_2O_3	Fe_2O_3	SO_3	CaO	Na_2O	P_2O_5	MgO	TiO_2		
1	0.6	wt%	10.369	16.386	0.607	2.956	11.192	0.062	0.575	0.155	0.004		
		mol%	0.648	1.024	0.038	0.185	0.700	0.004	0.036	0.010	0.000	2.6	
		Formula	0.859	1.809	0.074	0.163	1.854	0.023	0.042	0.028	0.000	7.0	Stratlingite & Melilite
2	0.8	wt%	11.748	14.678	0.556	1.840	12.040	0.090	0.490	0.175	0.013		
		mol%	0.734	0.917	0.035	0.115	0.753	0.006	0.031	0.011	0.001	2.6	
		Formula	0.988	1.645	0.066	0.103	2.024	0.019	0.020	0.018	0.001	7.0	Stratlingite & Melilite

$$Si_{0.859} \cdot Al_{1.809} \cdot Fe_{0.074} \cdot S_{0.163} \cdot Ca_{1.854} \cdot Na_{0.023} \cdot P_{0.042} \cdot Mg_{0.028} \cdot Ti_{0.000} \cdot O_7 \equiv 2CaO \cdot Al_2O_3 \cdot SiO_2$$

$$Si_{0.988} \cdot Al_{1.645} \cdot Fe_{0.066} \cdot S_{0.103} \cdot Ca_{2.024} \cdot Na_{0.019} \cdot P_{0.020} \cdot Mg_{0.018} \cdot Ti_{0.001} \cdot O_7 \equiv 2CaO \cdot Al_2O_3 \cdot SiO_2$$

B. Calculation from the quantitative analysis of the EDX spectra (CSH)

Analysis Group	Ash hydrated at W/A of		SiO_2	Al_2O_3	Fe_2O_3	SO_3	CaO	Na_2O	P_2O_5	MgO	TiO_2		
3	0.8	wt%	39.17	4.91	1.85	2.53	52.12	0.35	0.870	0.44	0.032		
			Si	**Al**	**Fe**	**S**	**Ca**	**Na**	**P**	**Mg**	**Ti**		
3	0.8	wt%	18.310	2.599	1.294	1.013	37.250	0.260	0.380	0.265	0.019		
		mol%	0.652	0.096	0.023	0.032	0.929	0.011	0.012	0.011	0.000		
		Mean molar ratios relative to Ca	0.701	0.104	0.025	0.034	1.000	0.012	0.013	0.012	0.000		
	Ash hydrated at W/A of		**Calculated O from**										
			SiO_2	**Al_2O_3**	**Fe_2O_3**	**SO_3**	**CaO**	**Na_2O**	**P_2O_5**	**MgO**	**TiO_2**		
3	0.8	wt%	20.860	2.311	0.556	1.517	14.870	0.090	0.490	0.175	0.013		
		mol%	1.304	0.144	0.035	0.095	0.929	0.006	0.031	0.011	0.001	**2.6**	
		Formula	0.893	0.132	0.032	0.043	1.273	0.019	0.020	0.018	0.001	**3.5**	CSH

C. Calculation from the quantitative analysis of the EDX spectra (ettringite)

Analysis Group	Ash hydrated at W/A of		SiO_2	Al_2O_3	Fe_2O_3	SO_3	CaO	Na_2O	P_2O_5	MgO	TiO_2		
4	0.6	wt%	7.98	10.23	3.81	27.93	44.12	0.44	6.02	1.38	0.03		
5	0.8		9.17	11.9	1.85	33.21	41.34	0.35	0.870	0.44	0.032		
			Si	**Al**	**Fe**	**S**	**Ca**	**Na**	**P**	**Mg**	**Ti**		
4	0.6	wt%	3.730	5.414	2.665	11.186	31.532	0.326	2.627	0.832	0.018		
		mol%	0.133	0.201	0.048	0.349	0.787	0.014	0.085	0.034	0.000		
		Mean molar ratios relative to Ca	0.169	0.255	0.061	0.443	1.000	0.018	0.108	0.044	0.000		
5	0.8	wt%	4.286	6.298	1.294	13.301	29.546	0.260	0.380	0.265	0.019		
		mol%	0.153	0.233	0.023	0.415	0.737	0.011	0.012	0.011	0.000		
		Mean molar ratios relative to Ca	0.207	0.317	0.031	0.563	1.000	0.015	0.017	0.015	0.001		
	Ash hydrated at W/A of		**Calculated O from**										
			SiO_2	**Al_2O_3**	**Fe_2O_3**	**SO_3**	**CaO**	**Na_2O**	**P_2O_5**	**MgO**	**TiO_2**		
4	0.6	wt%	4.250	4.816	1.145	16.744	12.588	0.114	3.393	0.548	0.012		
		mol%	0.266	0.301	0.072	1.047	0.787	0.007	0.212	0.034	0.001	2.7	
		Formula	0.179	1.324	0.315	2.302	5.192	0.042	0.249	0.100	0.001	**18.0**	Ettringite
5	0.8	wt%	4.884	5.602	0.556	19.909	11.794	0.090	0.490	0.175	0.013		
		mol%	0.305	0.350	0.035	1.244	0.737	0.006	0.031	0.011	0.001	2.7	
		Formula	0.209	1.545	0.153	2.746	4.880	0.019	0.020	0.018	0.001	**18.0**	Ettringite